

Electronic Supplementary Information (ESI)

**Ensemble effects of high entropy alloy for boosting alkaline water splitting
coupling with urea oxidation**

Jiace Hao[†], Jiale Li[†], Yinchao Zhu, Shuhui Sun, Shuanglong Lu, Mingliang Du and Han
Zhu*

Key Laboratory of Synthetic and Biological Colloids, Ministry of Education, School of
Chemical and Material Engineering, Jiangnan University, Wuxi, jiangsu 214122, P. R.
China.

E-mail: zhysw@jiangnan.edu.cn

Experimental

Materials

Cobalt chloride hexahydrate ($\text{CoCl}_2 \cdot 6\text{H}_2\text{O}$, AR), commercial Pt/C (20 wt%), bis(acetylacetonato)dioxomolybdenum ($\text{C}_{10}\text{H}_{14}\text{MoO}_6$, 97%) and potassium hydroxide (KOH, GR, 95%) were brought from Shanghai Macklin Biochemical Co., Ltd. Nickel chloride hexahydrate ($\text{NiCl}_2 \cdot 6\text{H}_2\text{O}$, AR), ruthenium chloride (RuCl_3 , AR) and urea ($\text{CH}_4\text{N}_2\text{O}$, AR) were supplied by Sinopharm Chemical Reagent Co., Ltd. N,N-dimethylformamide (DMF, $\geq 99.5\%$) was brought from Shanghai Titan Scientific Co., Ltd. Iron chloride hexahydrate (FeCl_3 , 98%) and Nafion117 solution (5 wt%) were acquired from Shanghai Aladdin Biochemical Technology Co., Ltd. Polyacrylonitrile (PAN, $M_w = 1.49 \times 10^5$, copolymerized with 10 wt% acrylate) was brought by Sinopec Shanghai Petrochemical Co., Ltd.

Synthesis of FeCoNiMoRu high entropy alloy nanoparticles supported on carbon nanofibers.

Initially, 0.5 mmol of FeCl_3 , 0.5 mmol of $\text{CoCl}_2 \cdot 6\text{H}_2\text{O}$, 0.5 mmol of $\text{NiCl}_2 \cdot 6\text{H}_2\text{O}$, 0.5 mmol of RuCl_3 , 0.5 mmol of $\text{C}_{10}\text{H}_{14}\text{MoO}_6$, and 2 g of PAN were dissolved in 22 g of DMF. After stirring for 12 h at room temperature, the homogeneous metal salts/PAN solution was acquired. Next, the as-prepared precursor solution was transferred into the syringes with stainless needles. And then the syringes were assembled into the electrospinning machine (YFSP-T, Tianjin Yunfan Technology Co., Ltd.) with an applied positive voltage of 18 kV on the needle, a negative voltage of 2 kV on the acceptor, an injection rate of 0.4 mL h^{-1} , and a distance between the collector and needle of 18 cm. Finally, the acquired nanofiber membranes were placed into the heating section of the home-built chemical vapor deposition (CVD) furnace and heated to $230 \text{ }^\circ\text{C}$ in air atmosphere with a heating rate of $5 \text{ }^\circ\text{C min}^{-1}$ and maintained for 3 hours. The nanofiber membrane was heated to $1000 \text{ }^\circ\text{C}$ under Ar atmosphere with a heating rate of $2 \text{ }^\circ\text{C min}^{-1}$ and maintained for 3 hours. The FeCoNiMoRu HEA/CNFs was obtained after the furnace cooling down to room temperature under Ar atmosphere. The control FeCoNiMo/CNFs, FeCoNiRu/CNFs, FeCoNi/CNFs, Ru/CNFs, Ni/CNFs and Mo/CNFs were also synthesized through the same process as that of FeCoNiMoRu HEA/CNFs. The amounts of each metal salts in the precursor solution were 0.5 mmol, respectively.

Electrochemical measurements

A CHI-660H workstation with a typical three-electrode system was used to carry out electrochemical measurements at $25 \text{ }^\circ\text{C}$. For HER and OER, 1.0 M KOH was used as the electrolyte, while a mixed electrolyte of 1.0 M KOH and 0.33 M $\text{CH}_4\text{N}_2\text{O}$ was utilized for UOR. Saturated calomel electrode (SCE) and a graphite rod were regarded as reference electrode and count electrode, respectively. And the SCE was calibrated before each test. The self-supported catalyst membranes were directly served as working electrode (WE). Pt/C (20 wt%) deposited on glassy carbon electrode (GCE) with diameter of 3 mm was applied as control sample for measurement. For the preparation of the electrocatalyst ink, 3 mg of electrocatalyst was dispersed in 1 mL

mixed solvent with a volume ratio of $V_{\text{isopropanol}}:V_{\text{water}} = 3:1$. After ultrasonication for 30 minutes, 25 μL Nafion117 solution was added. After another ultrasonication for 30 minutes, 5 μL electrocatalyst ink was casted on the surface of GCE and dried in air naturally. The potentials mentioned in the article were converted into the reversible hydrogen electrode (RHE) by the equation of $E_{\text{RHE}} = E_{\text{SCE}} + 0.244 + 0.059 \times \text{pH}$. All linear sweep voltammetry (LSV) curves were obtained at a scan rate of 2 mV s^{-1} with 95% iR-compensation. The UOR stability of the catalysts were estimated by chronoamperometric measurements in 1.0 M KOH with 0.33 M $\text{CH}_4\text{N}_2\text{O}$ for 90 h. Tafel plots were gained according to the Tafel equation of $\eta = a + b \log j$; where η , b , and j represent the overpotential, Tafel slope, and current density, respectively. In order to calculate the electrochemical active surface areas (ECSA) of the catalysts, the electrochemical double layer capacitances (C_{dl}) with various scan speed (v) were investigated from 0 to 120 mV s^{-1} . The C_{dl} can be calculated by the equation of $C_{\text{dl}} = \Delta j / 2 v$ ($\Delta i = j_a - j_c$, where j_a and j_c represent the positive and negative current, respectively). Electrochemical active surface area (ECSA) was estimated by the equation of $\text{ECSA} = A_{\text{geo}} * C_{\text{dl}} / C_s$, where A_{geo} is the geometric area of the working electrode and the specific capacitance value (C_s) was taken as 0.04 mF cm^{-2} .

Materials characterizations

The field-emission scanning electron microscope (SEM, Hitachi Regulus8100) at an acceleration voltage of 3 kV was applied to collect the FE-SEM images. The transmission electron microscope (TEM, FEI TalosF200x) at an acceleration voltage of 200 kV was used to record the TEM images. Energy dispersive X-ray spectroscopy (EDX) mapping images and line-scan EDX spectra were characterized via TEM. X-ray diffraction (XRD) patterns were obtained by a Smartlab 9kw advance powder X-ray $\text{Cu K}\alpha$ radiation diffractometer ($\lambda = 1.5406 \text{ \AA}$) in the range of $20 \sim 80^\circ$ at the scanning rate of 0.5 or $10^\circ \text{ min}^{-1}$, with the $\text{Cu K}\alpha$ source operating at 40 kV and 40 mA. Besides, we conducted the operando electrochemical Raman test in a home-made electrolyzer. Ag/AgCl electrode and Pt wire were used as the reference electrode and the counter electrode, respectively. Electrocatalysts dispersed on glass carbon electrode (GCE) were utilized as work electrode. The electrochemical processes was controlled by a CHI660E electrochemical workstation, and Raman spectrometer (inVia) used the laser wave-length of 785 nm.

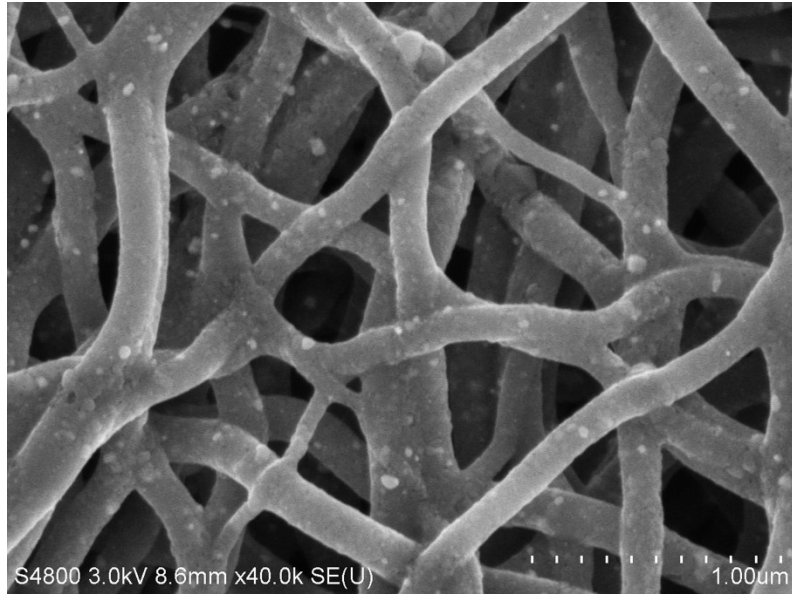


Figure S1. FE-SEM image of the FeCoNi/CNFs.

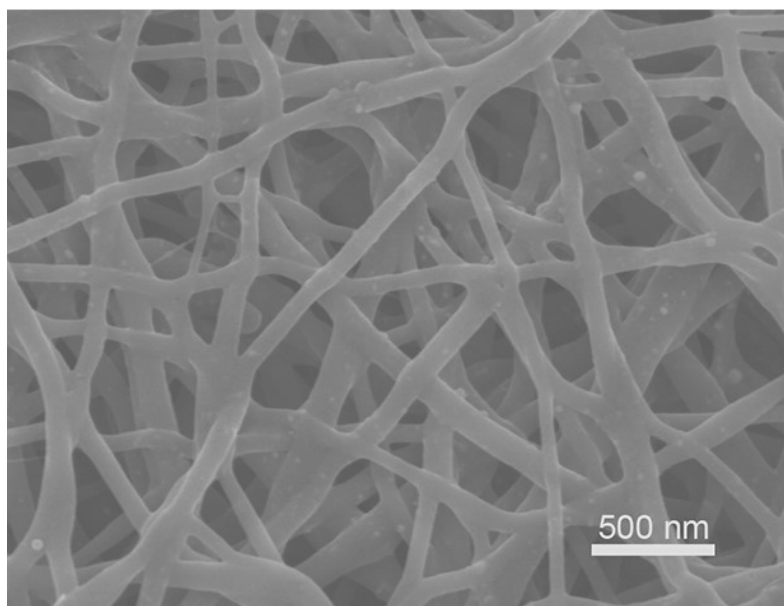


Figure S2. FE-SEM image of the FeCoNiMo/CNFs.

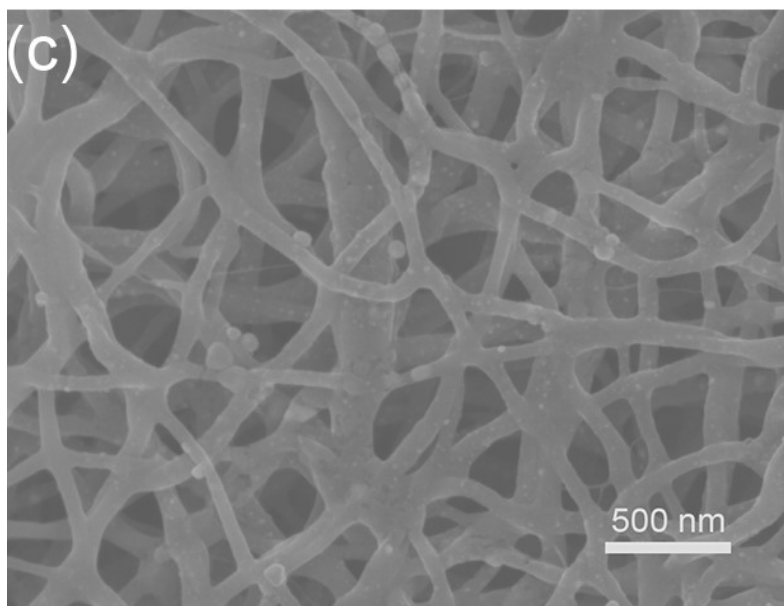


Figure S3. FE-SEM image of the FeCoNiRu/CNFs.

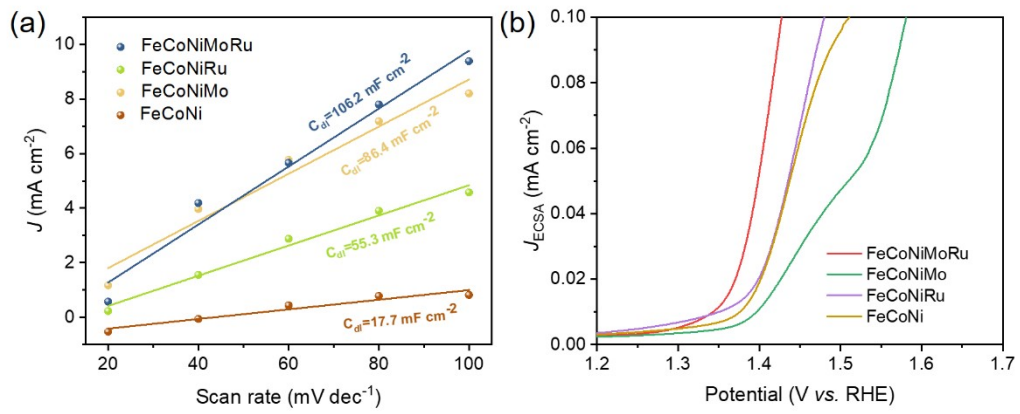


Figure S4. (a) Double-layer capacitance per geometric area (C_{dl}) and (b) the corresponding ECSA-normalized LSV curves of the as-prepared electrodes.

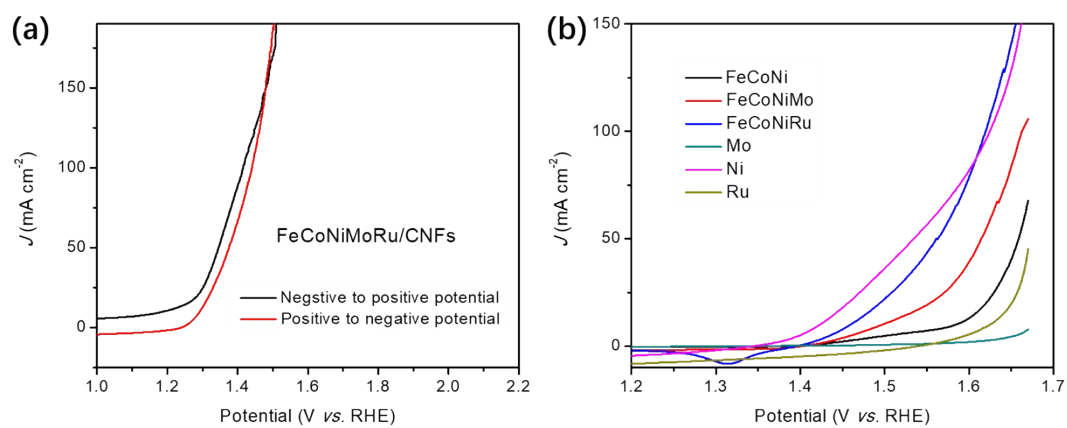


Figure S5. (a) LSV curves of FeCoNiMoRu/CNFs scanned from negative to positive potential (black) and from positive to negative potential (red). (b) Backward LSV scans (from positive to negative potential) of counterparts.

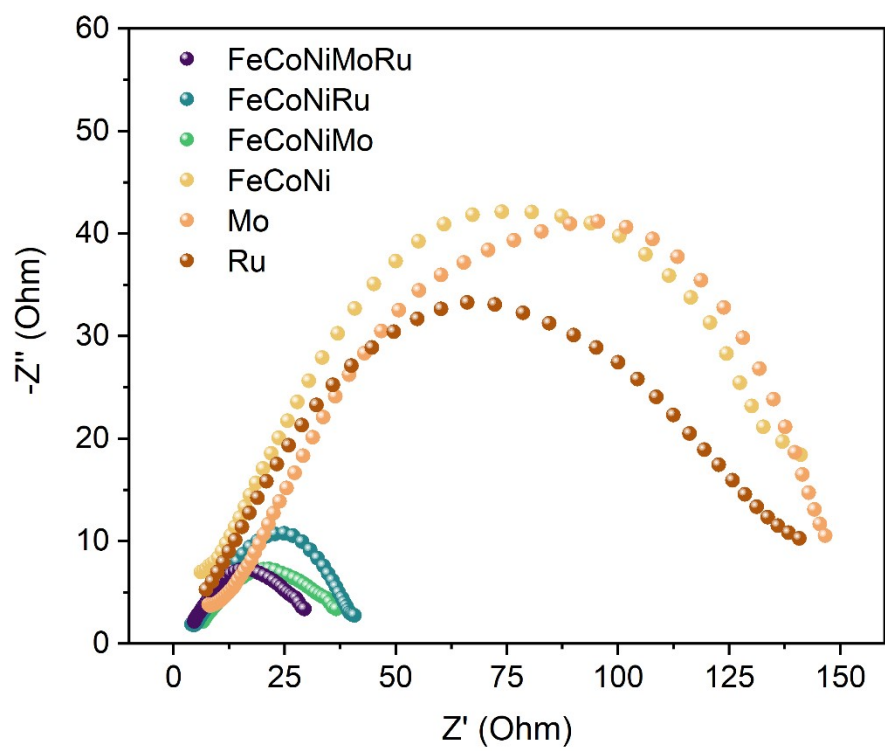


Figure S6. EIS spectra of FeCoNiMoRu/CNFs and controls.

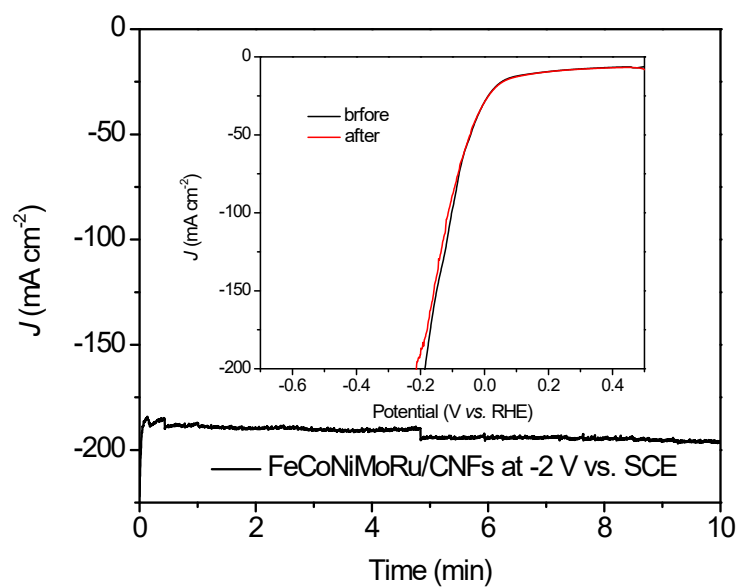


Figure S7. Chronoamperometric curve of FeCoNiMoRu/CNFs. The long-term chronoamperometry at highly negative potential was performed to guarantee that the electrocatalyst was fully reduced. The inset shows the LSV curves before and after chronoamperometry, and negligible difference can be observed.

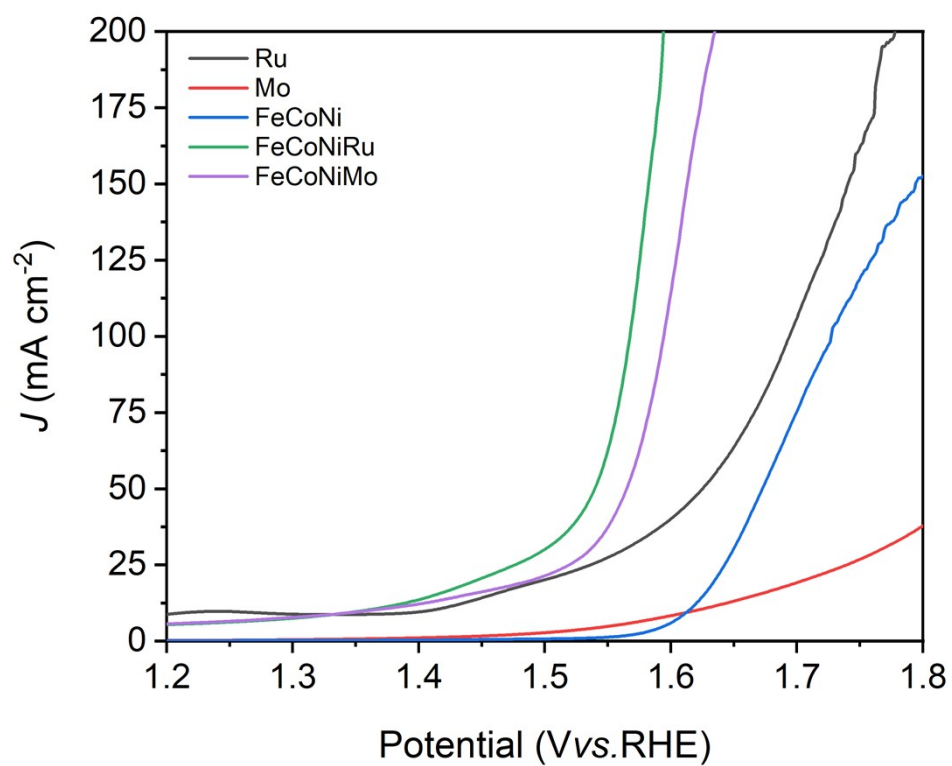


Figure S8. LSV curves of the as-prepared Ru/CNFs, Mo/CNFs, FeCoNi/CNFs, FeCoNiRu/CNFs and FeCoNiMo/CNFs used for OER in 1 M KOH.

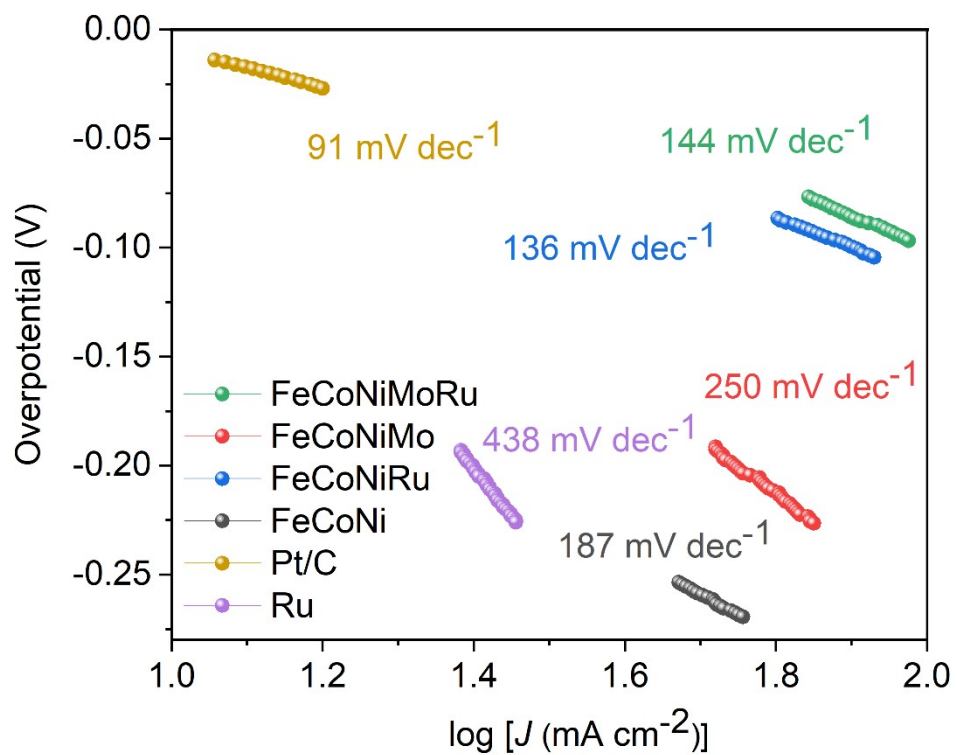


Figure S9. Tafel slopes of the as-prepared electrocatalysts for HER.

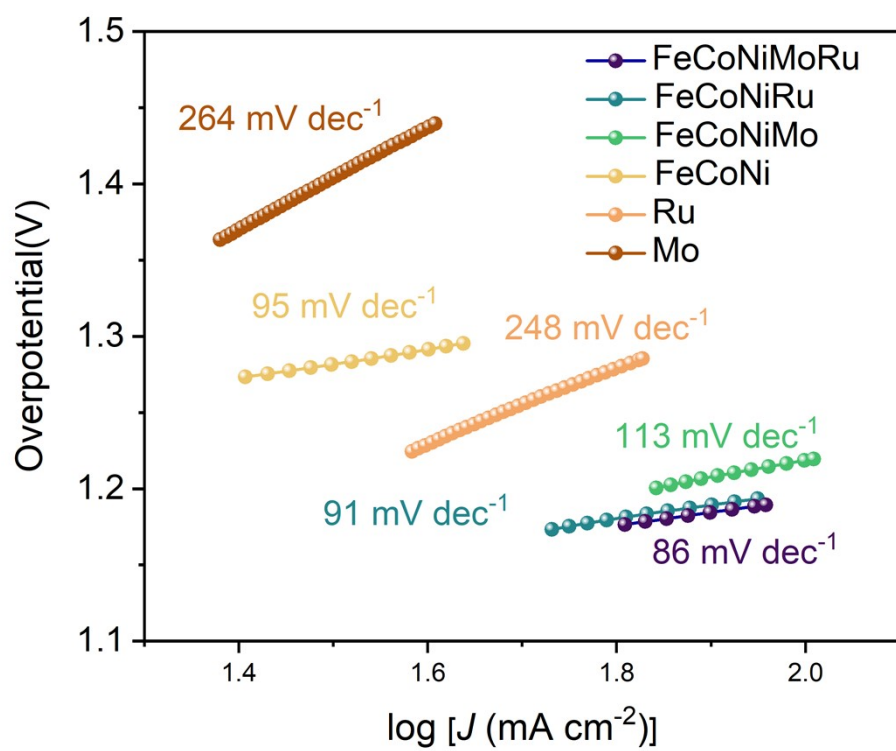


Figure S10. Tafel slopes of the as-prepared electrocatalysts for OER.

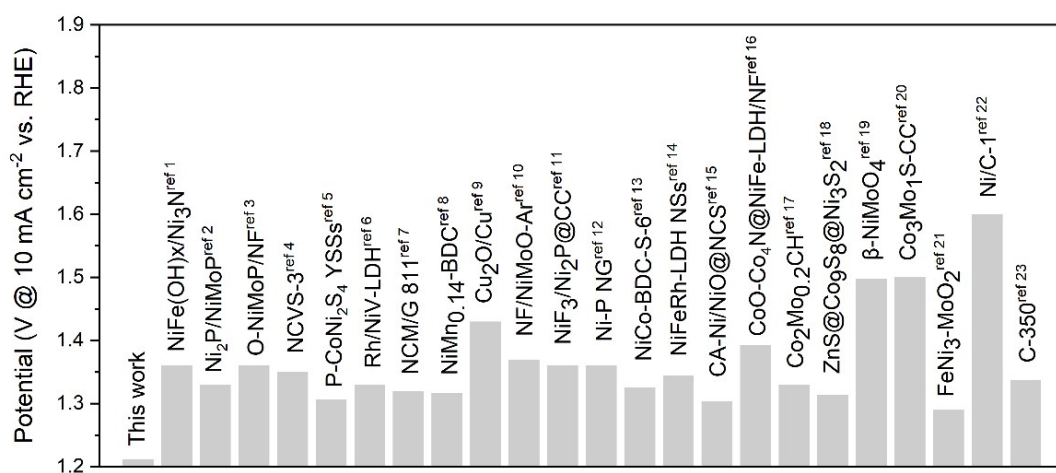


Figure S11. Comparison of UOR performance at 10 mA cm⁻² for different electrocatalyst.

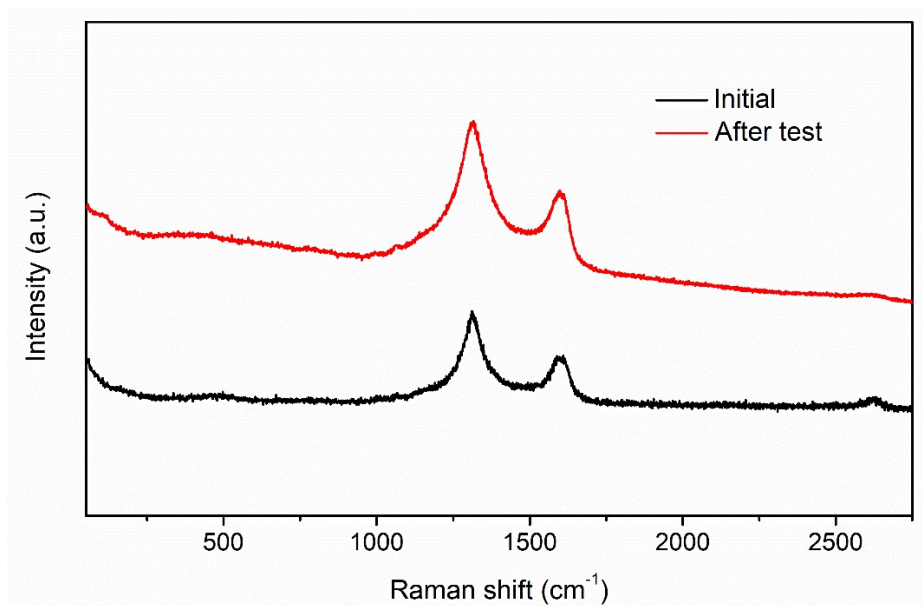


Figure S12. Raman spectra of FeCoNiMoRu/CNFs before and after used for UOR.

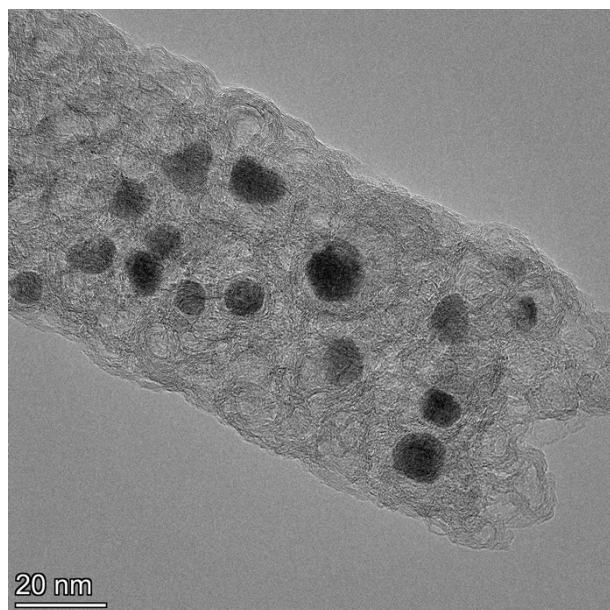


Figure S13. TEM image of the FeCoNiMoRu/CNFs after long-term stability test.

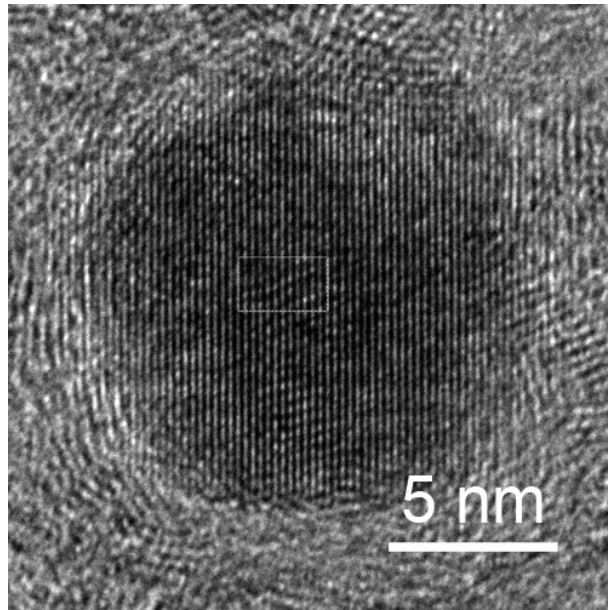


Figure S14. HRTEM image of the FeCoNiMoRu HEA NP supported on CNFs after long-term stability test.

Supplementary reference

1. H. J. Zhang, X. F. Meng, J. F. Zhang and Y. Huang, *ACS Sustainable Chem. Eng.*, 2021, **9**, 12584-12590.
2. T. Z. Wang, X. J. Cao and L. F. Jiao, *eScience.*, 2021, **1**, 69-74.
3. H. Yang, M. W. Yuan, Z. M. Sun, D. Wang, L. Lin, H. F. Li and G. B. Sun, *ACS Sustainable Chem. Eng.*, 2020, **8**, 8348-8355.
4. Z. J. Ji, Y. J. Song, S. H. Zhao, Y. Li, J. Liu and W. P. Hu, *ACS Catal.*, 2022, **12**, 569-579.
5. X. F. Lu, S. L. Zhang, W. L. Sim, S. Y. Gao and X. W. Luo, *Angew. Chem. Int. Ed.*, 2021, **60**, 22885-22891.
6. H. C. Sun, L. F. Li, H.-C. Chen, D. L. Duan, M. Humayun, Y. Qiu, X. Zhang, X. Ao, Y. Wu, Y. J. Pang, K.F. Huo, C. D. Wang and Y. J. Xiong, *Sci. Bull.*, 2022, **67**, 1763-1775.
7. W. Shi, X. J. Sun, R. Ding, D. F. Ying, Y. F. Huang, Y. X. Huang, C. N. Tan, Z. Y. Jia and E. H. Liu, *Chem. Commun.*, 2020, **56**, 6503-6506.
8. X. F. Xu, Q. M. D, H.-C. Chen, M. Humayun, D. L. Duan, X. Zhang, H. C. Sun, X. Ao, X. Y. Xue, A. Nikiforov, K. F. Huo, C. D. Wang and Y. J. Xiong, *Research*, 2022, **2022**, 9837109.
9. Q. Hu, B. Zhu, G. M. Li, X. F. Liu, H. P. Yang, Chris D. Sewell, Q. L. Zhang, J. H. Liu, C. X. He and Z. Q. Lin, *Nano Energy.*, 2019, **66**, 104194.
10. Z.-Y. Yu, C.-C. Lang, M.-R. Gao, Y. Chen, Q.-Q. Fu, Y. Duan and S.-H. Yu, *Energy Environ. Sci.*, 2018, **11**, 1890.
11. K. L. Wang, W. Huang, Q. H. Cao, Y. J. Zhao, X. J. Sun, R. Ding, W. W. Lin, E. H. Liu and P. Gao, *Chem Eng J.*, 2022, **427**, 130865.
12. C. Q. Pei, S. Q. Chen, T. C. Zhao, M. Li, Z. T. Cui, B. A. Sun, S. G. Hu, S. Lan, H. Hahn and T. Feng, *Adv. Mater.*, 2022, **34**, 2200850.
13. X. Ao, Y. Gu, C. J. Li, Y. Wu, C. H. Wu, S.Y. Xun, A. Nikiforov, C. I. Xu, J. Z. Jia, W. W. Cai, R. G. Ma, K. F. Huo and C. D. Wang, *Appl. Catal. B-Environ.*, 2022, **315**, 121586.
14. H. C. Sun, W. Zhang, J.-G. Li, Z. S. Li, X. Ao, K.-H. Xue, K. K. Ostrikov, J. Tang, C. D. Wang, *Appl. Catal. B-Environ.*, 2021, **284**, 119740.
15. X. Xu, X. Hou, P. Du, C. Zhang, S. Zhang, H. Wang, A. Toghan and M. Huang, *Nano Research.*, 2022, **15**, 7124-7133.
16. X. T. Wu, L. L. Li, J. Pan, X. Wang, H. B. Zhang, S. Y. Song, H. J. Zhang, *Materials Lab.*, 2022, **1**, 20220009.
17. S. Y. Zheng, H. Ye. Qin, X. J. Cao, T. Z. Wang, W. B. Lu, L. F. Jiao, *J. Energy Chem.*, 2022, **70**, 258-265.
18. X. Q. Du, Y. Y. Ding, X. S. Zhang, *GEE.*, 2021, in press.
19. K. L. Hu, S. Jeong, G. Elumalai, S. Kukunuri, J. Fujita and Y. Ito, *ACS Appl. Energy Mater.*, 2020, **3**, 7535-7542.
20. P. Li, Z. H. Zhuang, C. Du, D. Xiang, F. Q. Zheng, Z. W. Zhang, Z. Y. Fang, J. H. Guo, S. Y. Zhu and W. Chen, *ACS Appl. Mater. Interfaces.*, 2020, **12**, 40194-40203.
21. Q. L. Xu, T. Q. Yu, J. L. Chen, G. F. Qian, H. N. Song, L. Luo, Y. L. Chen, T. Y. Liu, Y. Z. Wang and S. B. Yin, *ACS Appl. Mater. Interfaces.*, 2021, **13**, 16355-16363.
22. C. J. Gu, G. Y. Zhou, J. Yang, H. Pang, M. Y. Zhang, Q. Zhao, X. F. Gu, S. Tian, J. B.

Zhang, L. Xu and Y. W. Tang, *Chem. Eng. J.*, 2022, **443**, 136321.

23. S. N. Hu, S. Q. Wang, C. Q. Feng, H. M. Wu, J. J. Zhang and H. Mei, *ACS Sustainable Chem. Eng.*, 2020, **8**, 7414–7422.